ARTICLE TYPE www. rsc.org/xxxxxx | XXXXXXXX

A General Mechanism for Controlling Thin Film Structures in All-Conjugated Block Copolymer:Fullerene Blends†

Rajeev Dattani,[a,b] James H. Bannock,[a,c] Zhuping Fei,[a,c] Roderick C. I. MacKenzie,[d] Anne A. Y. Guilbert,[a,b] Michelle S. Vezie,[e] Jenny Nelson,[a,e] John C. de Mello,[a,c] Martin Heeney,[a,c] João T. Cabral,[a,b] and Alisyn J. Nedoma*[a,b]

Received Xth XXXXXXXXXX 20XX, Accepted Xth XXXXXXXXX 20XX
First published on the web Xth XXXXXXXXXX 200X
DOI: 10.1039/b000000x

Block copolymers have the potential to self-assemble into thermodynamically stable nanostructures that are desirable for plastic electronic materials with prolonged lifetimes. Fulfillment of this potential requires the simultaneous optimisation of the spatial organisation and phase behaviour of heterogeneous thin films at the nanoscale. We demonstrate the controlled assembly of an all-conjugated diblock copolymer blended with fullerene. The crystallinity, nanophase separated morphology, and microscopic features are characterised for blends of poly(3-hexylthiophene-*block*-3-(2-ethylhexyl) thiophene) (P3HT-*b*-P3EHT) and phenyl-C61-butyric acid methyl ester (PCBM), with PCBM fractions varying from 0 - 65 wt%. We find that PCBM induces the P3HT block to crystallise, causing nanophase separation of the block copolymer. Resulting nanostructures range from ordered (lamellae) to disordered, depending on the amount of PCBM. We identify the key design parameters and propose a general mechanism for controlling thin film structure and crystallinity during the processing of semicrystalline block copolymers.

1 Introduction

Plastic electronics promise to revolutionise the way we harvest, store, and use energy by enabling the production of cheap, flexible devices via established high-throughput processing techniques. The stability and lifetime of plastic electronic materials remains one of the greatest challenges for their commercialisation[1], with current lifetimes barely reaching 5000 hours[2]. The greatest cause for loss of performance in organic solar cells (OSC's) is morphological instability, a result of out-of-equilibrium structures that evolve during heating-cooling cycles inherent to operation. Block copolymers are well-known for their ability to self-assemble into thermally stable nanostructures[3] commensurate with OSC requirements, 5-100 nm. The hierarchical structuring of polymer crystals within an ordered copolymer suprastructure is thought to be advantageous to the performance of thin film devices[4,5]. However, the performance of block copolymer-based OSC's has remained stubbornly low, due to the challenges associated with the multi-parameter morphological control

† Electronic Supplementary Information (ESI) available: [Included are graphs and images that support the main text and details of the GIWAXS reduction]. See DOI: 10.1039/b000000x/

*anedoma@imperial.ac.uk
[a] *Centre for Plastic Electronics, Imperial College London, London SW7 2AZ, UK.*
[b] *Department of Chemical Engineering, Imperial College London, London SW7 2AZ, UK.*
[c] *Department of Chemistry, Imperial College London, London SW7 2AZ, UK.*
[d] *Faculty of Engineering, University of Nottingham, Nottingham NG7 2RD, UK.*
[e] *Department of Physics, Imperial College London, London SW7 2AZ, UK.*

and, in particular, the incorporation of a mobile, crystallisable, fullerene phase. In this paper we demonstrate the controlled self-assembly of a diblock copolymer based on the well-studied donor/acceptor system of P3HT blended with PCBM, and provide a rationale to engineer the nano-morphology, crystallinity, orientation and segregation.

Diblock copolymers form phase separated nanostructures that can be scaled and shaped by controlling the molecular weight and architecture of the copolymer[3]. When one or both blocks of a diblock copolymer are semicrystalline, the kinetics of equilibrium phase separation compete with crystallisation[6–8]. Careful selection of the processing conditions can result in polymer crystals that are confined within the domains of the copolymer nanostructure[9–13].

This study aims to identify the key parameters and processing conditions needed to engineer the structure of thin films blends of a semicrystalline diblock copolymer and fullerene. The diblock copolymer selected for this study, poly(3-hexylthiophene-*block*-3-(2-ethylhexyl) thiophene), hereafter denoted P3HT-*b*-P3EHT, is shown in Fig. 1, and the fullerene is phenyl-C61-butyric acid methyl ester (PCBM). These materials were chosen based on the canonic P3HT:PCBM OSC. The diblock copolymer is symmetric and forms a lamellar nanophase separated structure, found to enhance polymer crystallisation relative to morphologies with higher curvature (e.g. cylinders or microemulsions)[10]. Only the P3HT block can crystallise, and PCBM cannot intercalate into the pure phase polymer crystal[14,15]. The amorphous P3EHT block is designed to preferentially dissolve the PCBM in a spatially confined domain that is directly adjacent to semicrystalline P3HT, producing a fine degree of phase separation that is desirable for OSC's.

Three distinct kinetic processes can compete in our study: (i) crystallisation of one block of the copolymer, (ii) microphase separation of the fullerene from the copolymer, including crystallisation of the fullerene, and (iii) microphase separation of the blocks within the copolymer. A low molecular weight block copolymer is selected for this study in order to produce domain sizes 10 nm, with the consequence that the copolymer is above the order-disorder transition at all temperatures studied. Microphase separation proceeds only via crystallisation of one block, a regime known as breakout crystallisation, and favours lamellar nanostructures[6–8,16]. The resulting film structures are the processing-dependent result of kinetic competition between polymer and fullerene crystallisation.

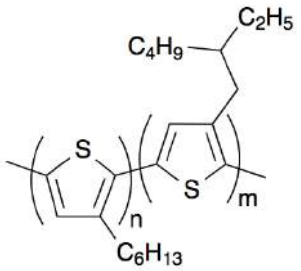

Fig. 1 Chemical structure of symmetric P3HT-*b*-P3EHT, $n = 33$ and $m = 28$.

In the current study, we examine a series of 100 nm thick films of P3HT-*b*-P3EHT blended with PCBM, in which the PCBM content varies from 0 - 65 wt%. Thermal processing is used to anneal the semicrystalline P3HT block, and thereby drive nanostructured ordering. PCBM monotonically increases the crystalline fraction of P3HT, and has an ordering effect on the diblock copolymer lamellae at intermediate concentrations (35 - 40 wt%). At high loadings of PCBM (50 wt%) the copolymer structure disorders. Micron-scale undulations of the film surface evolve as the PCBM concentration increases. Blends above a threshold concentration of PCBM in P3HT-*b*-P3EHT, $x_{rod} \sim 22 \pm 12$ wt%, exhibit microscopic rods of PCBM along with the onset of x-ray diffraction peaks indexed to PCBM. On the basis of these observations, we propose a general mechanism describing the evolution of nano-

and microstructures towards the rational optimisation of processing for semicrystalline block copolymer:small molecule blends.

2 Experimental section

2.1 Materials

Phenyl-C61-butyric acid methyl ester (PCBM) from Solenne, chlorobenzene 99.9% AnalR NORMAPUR from VWR, an aqueous solution of PEDOT:PSS (Clevios PVP. AL 4083) from Heraeus, and clean dry nitrogen from BOC were used as received. Silicon wafers <100>were purchased from Compart Technologies.

2.2 Polymer synthesis and characterisation

The family of poly-3-alkylthiophenes were synthesised by Grignard metathesis. Poly-3-hexylthiophene (P3HT) (M_w 20 kg/mol, PDI 1.8, RR 89 % by integration of the methylene region, not corrected for end-group effects) and poly-3-(2-ethylhexyl) thiophene (P3EHT) (M_w 50 kg/mol used for thermal characterisation and M_w 16 kg/mol, PDI 1.7, RR 90 %, by integration of the ring proton region, not corrected for end-group effects, used for optical characterisation) were prepared using the Grignard metathesis as previously reported[17,18]. Both materials were prepared at a reaction temperature of 45 °C with a Ni(dppp)Cl_2 catalyst loading of 2.7 mol%. P3HT-*b*-P3EHT (M_w 11 kg/mol, PDI 1.8, 3-HT:3-EHT of 54:46 by integration of the regioregular methylene signals from each species, see ESI) was prepared using an analogous method to that of Zhang et al.[19], as described in Section S1.1 of the ESI. All three polymers were purified by Soxhlet extraction; first with methanol (24 hours) to remove excess monomer and salt byproducts, and followed by chloroform (1 hour) to extract the polymer from any remaining insoluble impurities.

2.3 Solution preparation

A stock solution of the diblock copolymer in chlorobenzene was left stirring for 12 hours at 40 °C, and PCBM in chlorobenzene was left stirring for 12 hours at 20 °C. Both stock solutions were filtered with a 0.2 μm PTFE filter prior to blending. Binary blends of P3HT-*b*-P3EHT and PCBM were prepared with PCBM fractions ranging from 0 to 65 wt%. The final composition of each blend was calculated from the mass of each solution transferred. All blends were concentrated by heating to 60 °C under a stream of 1 μm-filtered clean, dry nitrogen until the final concentration of dissolved polymer was 1.2 wt%. The precise composition of each blend is listed in ESI Table S2. Sample names are given by BXX to denote that blends are binary, composed of P3HT-*b*-P3EHT and PCBM, with XX weight percentage PCBM.

2.4 Thin film fabrication

Silicon wafers were blown clean with filtered dry nitrogen. The polished surface was exposed to UVO for 15 minutes in a Novascan UV ozone cleaner and left in the ozone chamber for an additional 30 minutes to develop a layer of silicon oxide. PEDOT:PSS was filtered through a 0.2 μm hydrophilic filter directly onto the clean silicon wafer, and spin coated at 1500 RPM for 1 minute followed by 3000 RPM for 30 seconds to improve drying. The wafers were heated to 140 °C under vacuum for 1 hour, and allowed to remain under vacuum for an additional 3 hours to ensure drying. This resulted in a 45 nm thick PEDOT:PSS layer as measured by atomic force microscopy. The PEDOT:PSS-coated substrates were cut to size, cleaned with nitrogen, and stored on a hotplate at 60 °C to prevent the absorption of ambient water. The diblock copolymer solution was applied to the prepared substrates using an RK Printer wire bar coater. The wire bar was set 300 μm above the substrate (using a folded piece of paper to make the gap), the bottom platten was heated to 60 °C, and the speed of the wire bar was 80 mm/sec. Polymer solutions (1.2 wt% polymer) were heated to 50 °C to ensure homogeneity, and a 10 μL bead of solution was spread across the top of the substrate and immediately coated. This resulted in diblock copolymer films of thickness 100 $\pm$ 5 nm atop the 45 nm thick PEDOT:PSS layer. Films

were annealed at 50 mbar in a Memmert vacuum oven and left under vacuum until they had cooled to 50 °C to prevent oxidation. Prior to characterisation, the annealed films were stored in a dark box with desiccant to prevent humidification of the PEDOT:PSS under layer.

2.5 Grazing incidence wide angle x-ray scattering

Grazing incidence wide angle x-ray scattering measurements (GIWAXS) were carried out at beam line I07 Diamond (RAL, Didcot). The grazing incidence angle, α_i, was varied from 0 to 0.3°, an incident energy of 8 keV was used, and the sample was continuously translated in the beam to minimise degradation at a single spot. The raw data were masked to eliminate gaps between detector panels and imperfect pixels, and the q-calibration was made using a silver behenate standard. The grazing incidence geometry and definition of the scattering vector q are shown in ESI Fig. S5. A detailed description of the data reduction procedure is provided in the ESI Section S2.

Two-dimensional GIWAXS spectra were collected for the series of blended thin films ranging from pure diblock copolymer to pure PCBM. Unless otherwise noted, films were annealed for 6 hours at 200 °C. The maximum scattered intensity for all films occurred at an incident angle α_i = 0.18°, roughly in between the critical angles of the polymer film and the silicon substrate (∼0.14 and ∼0.22°, respectively). Although full rocking curves were obtained for angles from 0 - 0.3°, only the data at 0.18° is considered below.

2.6 Surface characterisation

Optical micrographs were acquired using an Olympus BX41M-LED reflectance mode microscope equipped with an Allied GX1050C colour camera. The evolution of microscale structure was examined *in situ* for several samples using a THMS 600 Linkam Thermal Cell mounted onto the microscope stage and a 50x long focussing length objective. The Linkam sample chamber was flushed and sealed under nitrogen to minimise oxidation of the samples. Care was taken to translate the sample on the microscope stage to ensure that no light-exposed region was observed twice.

Atomic force microscopy (AFM) measurements were made using a Bruker diInnova microscope in tapping mode. Height and phase data were collected for all samples. For microscopically rough films, a smooth region was chosen, away from any microscopic PCBM crystals. Discrete Fourier Transforms (DFT's) of the amplitude of the AFM phase image, shown in Supplemental Fig. S8, were radially integrated to compute the characteristic length scales that emerge as peaks.

2.7 Differential scanning calorimetry

A Mettler Toledo DSC886^e differential scanning calorimeter (DSC) was used to characterise the thermal properties of bulk (∼ 5 mg) samples. Nitrogen gas was flowed through the sample furnace during measurement to minimise sample oxidation, and the pan lids were punctured with a needle to allow contact with the inert gas.

3 Results and discussion

3.1 Thermal characterisation of pure components

DSC was used to identify the relevant transition temperatures: the melting point, T_m, melt crystallisation temperature, T_c, and glass transition, T_g. The results are summarised in Table 1 and the DSC profiles are shown in Fig. 2a. Low temperature DSC profiles for each species detail the T_g and side chain melting transitions in ESI Fig. S4.

Thermal cycling yielded sharp melting and crystallisation peaks for P3HT, with a similar heat capacity as reported by Thurn-Albrecht et al.[20] and transition temperatures consistent with the literature[18,20–22]. P3EHT did not exhibit any peaks

Sample	T_g (°C)	$T_{c,cyc}$ (°C)	$T_{m,cyc}$ (°C)	T_m (°C)	ΔH_m (J g^{-1})
P3HT (20 Kg/mol)	-9	183	217	220	92.6
P3EHT (50 Kg/mol)	9	—	—	85	18.0
P3HT-*b*-P3EHT (11 Kg/mol)	-2	156	221	228	9.77
PCBM	130	256	291	290	22.0

Table 1 Thermal characteristics of each polymer species measured in DSC using a ramp rate of 10 °C/min. $T_{m,cyc}$ and $T_{c,cyc}$ were measured from the second heating-cooling cycle, whilst T_m and ΔH_m were both measured during the first heating ramp following a standard anneal. P3EHT did not exhibit any peaks during cycling in the range -50 to 300°C. Details of the T_g measurement are available in ESI Fig. S4.

during cycling, however, ageing for one day at 25°C reproducibly resulted in a split melting peak spanning the range 40 - 85°C (see ESI Fig. S4). The two P3EHT endotherms are consistent with the results of Ho et al.[18] who inferred the melting of two distinct crystal structures observed using WAXS. The diblock copolymer exhibits two broad endotherms between 160 and 221°C. The highest melting point during cycling, $T_{m,cyc}$, is 221°C, in good agreement with T_m = 222°C measured for an $n = 36$ P3HT oligomer[23]($n = 33$ for the P3HT block of the copolymer). The low-temperature endotherm is likely related to melting and reorganisation of the semicrystalline P3HT block, rather than melting of the P3EHT block, as it occurs nearly 80°C above the T_m of neat P3EHT.

Thermal annealing at T_{anneal} = 200 °C, intermediate between T_m and T_c of the block copolymer, was selected to promote reorganisation and coarsening of the P3HT crystals. The "standard anneal" used is 6 hours at 200°C followed by a slow cooling as shown in Figure 2b. Following the standard anneal, the diblock copolymer exhibits only one melting peak, due to the P3HT block, confirming that the low temperature endotherm observed during cycling is due to reorganisation. The solid black lines in Figure 2a show the first heating run for samples exposed to the standard anneal. Noticeably, all crystalline samples exhibit sharper peaks after the anneal due to a higher degree of crystal ordering.

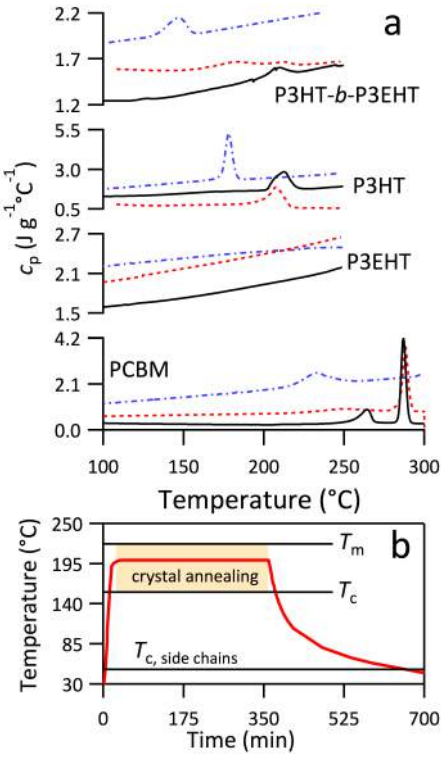

Fig. 2 Thermal characterisation of P3HT-*b*-P3EHT, P3HT, P3EHT, and PCBM. (a) DSC heat capacity profiles measured at 10°C/min for the second heating cycle (- - -), second cooling cycle (- · -), and first heating cycle following a standard anneal (——). (b) Thermal profile for a "standard anneal" with relevant transition temperatures labeled.

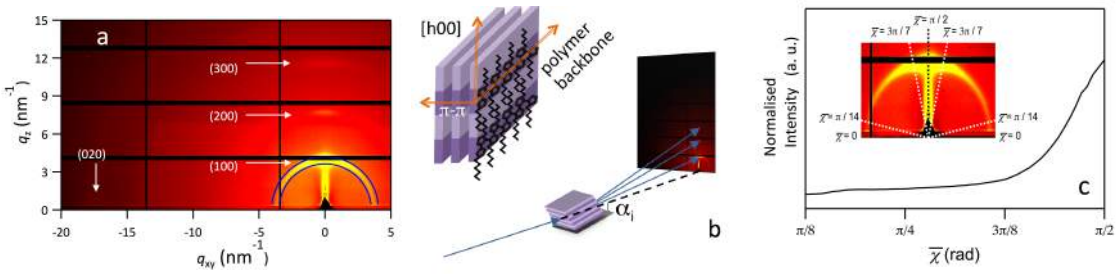

Fig. 3 GIWAXS spectra of a P3HT film on PEDOT:PSS. (a) The corrected 2-D spectrum with diffraction peaks labeled. The integration region is demarcated with solid blue lines (—). (b) Schematic of the chain packing for a single edge-on P3HT crystal in the GIWAXS geometry (c) Azimuthal integration of the (100) diffraction ring in (a). The inset details the polar coordinate system used.

3.2 Crystallinity measured by GIWAXS

GIWAXS is used to quantify the relative degree of polymer crystallinity between samples in the series of P3HT-*b*-P3EHT:PCBM thin films. All blends exhibit diffraction peaks characteristic of highly oriented P3HT crystals, and blends exceeding x_{rod} also exhibit PCBM diffraction peaks. A representative 2-D spectrum for the neat P3HT homopolymer is shown in Fig. 3a with the lattice reflections indicated. The strong anisotropy of diffraction arcs is consistent with a monoclinic crystal lattice[24] oriented "edge-on" with respect to the substrate[14,25–28], as illustrated in Figure 3b. The complete set of 2-D spectra for the blends is shown in ESI Fig. S6.

The P3EHT block of the copolymer appears to be completely amorphous as there is no detectable diffraction peak, consistent with the lack of a P3EHT endotherm in the copolymer DSC profile. The P3HT block of the neat diblock copolymer exhibits weak diffraction peaks because only half of the sample volume (the P3HT block) can crystallise.

The degree of crystallinity is traditionally determined by measuring the areas under diffraction peaks. This analysis is not possible with our data because an inopportune gap between the detector panels coincides with the first order [h00] peak. We developed an alternative approach to quantify the crystallinity of samples relative to one another, based on the observation that P3HT crystals scatter anisotropically out of the plane of the film whilst PCBM crystals scatter isotropically[29]. Integrating the (100) peak azimuthally, as shown by the blue dotted lines in Figure 3a, yields a partial pole figure like that in Figure 3c. The 2-D profiles are symmetric about $q_z = 0$, so an average azimuthal angle, $\bar{\chi}$, integrates areas on both sides of the detector to improve statistics. The difference in magnitude between scattering out of the plane of the film ($\bar{\chi} = \pi/2$) and in the plane of the film ($\bar{\chi} = 0$) is directly related to the total volume of P3HT crystals.

Partial pole figures for each sample, normalised to account for the slightly different scattering volumes, are shown in Fig. 4a. The fraction of scattering due to oriented P3HT crystals is defined as $I_{xtal} = \int_{3\pi/7}^{\pi/2} I \mathrm{d}\bar{\chi}$. I_{xtal} is plotted for each blend in Fig. 4b, showing a nearly constant degree of crystallinity over a wide range of concentrations despite the fact that the overall fraction of copolymer is decreasing in these samples. Fig. 4c shows I_{xtal} normalised by the weight fraction of the P3HT block in the sample, x_{P3HT}. The fraction of the P3HT block that crystallises, relative to the total mass of P3HT in the sample (i.e. excluding the mass of the P3EHT block), is seen to increase linearly with the fraction of PCBM. There is

precedent for the observation that PCBM monotonically increases the size of polymer crystals in P3HT:PCBM blends[25]. The surprising result is that the effect does not saturate at x_{rod}, suggesting a kinetic rather than thermodynamic origin for this phenomenon, as discussed in the General Mechanism section.

Two samples were studied without any thermal annealing and are shown by the filled circles in Fig. 4b. The neat diblock copolymer exhibits nearly the same degree of crystallinity before and after annealing, indicating rapid crystallisation during film drying. The blended film, B65, does not exhibit any measurable crystallinity as cast but crystallises extensively upon annealing. As observed in P3HT:PCBM films prepared from chlorobenzene[30], PCBM is known to suppress the crystallinity of P3HT in drying films. Together, these results indicate a mechanistic transition from solution crystallisation to cold crystallisation of P3HT as the fraction of PCBM increases in the annealed blends.

3.3 Nanophase separation

Nanophase separation of the diblock copolymer is examined at the top interface of each film using phase contrast AFM (Fig. 5). The corresponding height images are duplicated alongside these images in ESI Fig. S8. The patchy, light-coloured regions comprise P3HT-rich nanophase domains with a higher elastic modulus than the P3EHT domains due to the presence of polymer nanocrystals. At low concentrations of PCBM the structures are disordered, evolving into clear grains with high registry for 35-40 wt% PCBM, and then disordered drop-like and sponge-like structures in blends with 50 and 65 wt% PCBM, respectively. To quantify these trends, we measure the average correlation length between domains, d_λ.

Radially integrated DFT's for each blend are shown in Fig. 6a, the full 2-D spectra are in ESI Fig. S8. The $q*$ value corresponding to d_λ is

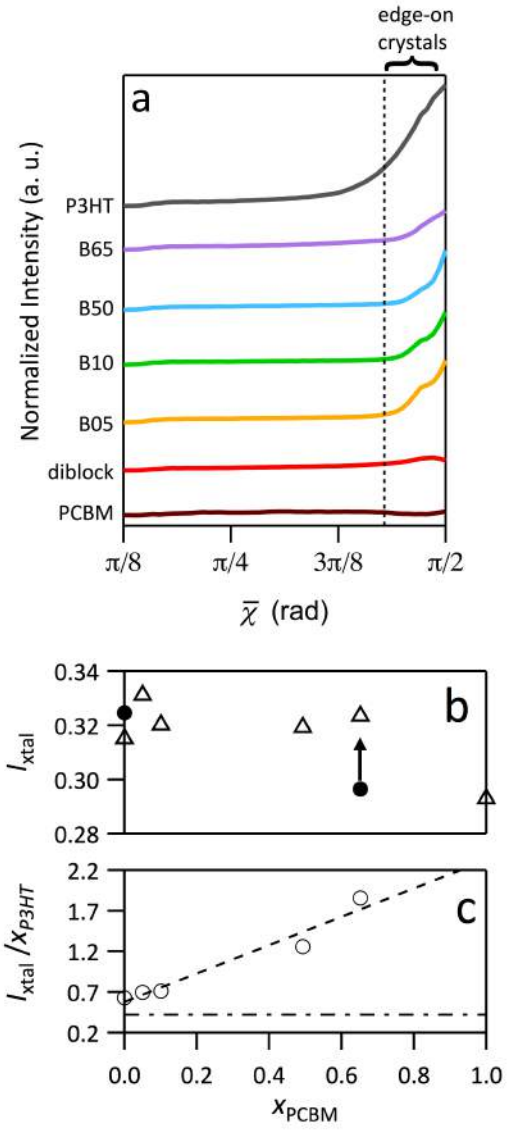

Fig. 4 GIWAXS analysis of P3HT crystallinity in films comprising P3HT-*b*-P3EHT and PCBM. (a) Azimuthal integrations of the (100) diffraction ring of P3HT show an upturn due to edge-on crystals. The region between the vertical dashed line and $\pi/2$ was integrated to obtain I_{xtal}. (b) The fraction of (100) scattering due to edge-on P3HT crystals, I_{xtal} (△), scales with P3HT crystallinity. Values for two as cast samples are shown (●). (c) I_{xtal} / x_{P3HT} (○), the crystalline fraction relative to the total amount of crystallisable polymer, versus PCBM fraction. A linear fit to the data (- - -) and the value for pure P3HT(- · -) are shown.

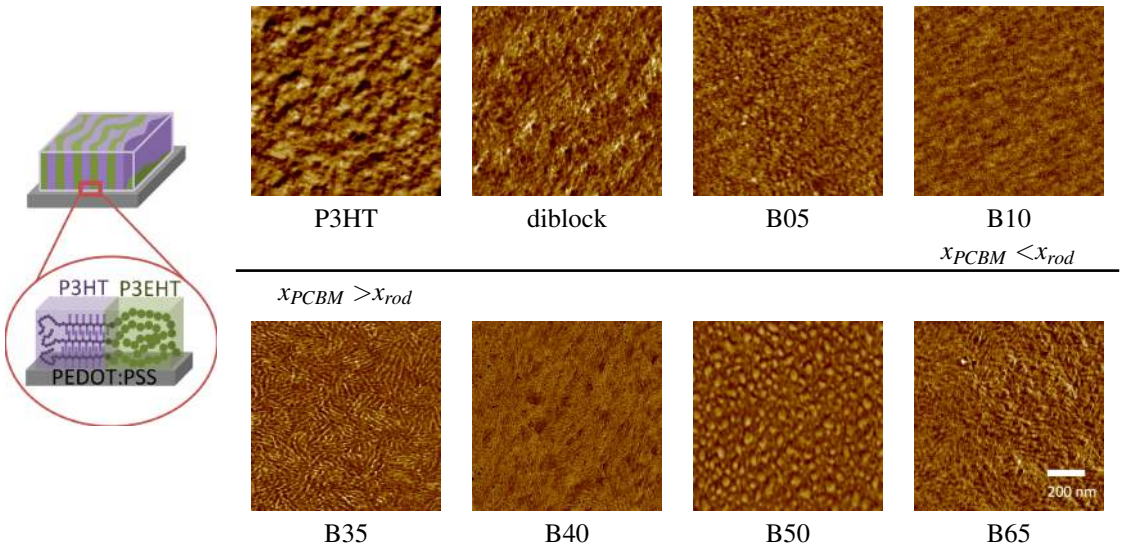

Fig. 5 Nanostructures in P3HT-*b*-P3EHT:PCBM thin films. Tapping mode AFM phase contrast images 1 x 1 μm are shown for thin film samples following a standard anneal. The colour map is scaled arbitrarily for visible contrast. The schematic on the left shows the proposed morphology of the ordered diblock copolymer lamellae in blends B35 and B40.

indicated with an arrow for blends exhibiting a distinct correlation peak. Values for $d_\lambda = \pi/q*$ are shown in Fig. 6b (NB the relationship between d_λ and $q*$ differs from that of a scattering experiment due to the discrete nature of the DFT). At low concentrations of PCBM d_λ is relatively constant, but increases for blends above 35 wt% PCBM.

The nanostuctures in B05 and B10 exhibit features distinct from the neat diblock copolymer, but are disordered. Clear, ordered structures, likely to be edge-on lamellae, appear when the PCBM fraction is greater than x_{rod}. The width of the lamellar domains in B35 and B40 is 14 nm, far smaller than the length expected for a fully extended P3HT block with n = 33 ($\sim$ 33 nm). Conventionally, oligomers of this size do not exhibit chain folding, so it is likely that only a portion of the P3HT block is crystallised and the remainder is amorphous.

The large, droplet-like structure of B50 appears to comprise of P3HT-rich islands in an amorphous matrix. The P3HT block constitutes only 25% of the total mass of B50, in the same range where lamellar to microemulsion transitions are observed in block copolymer blends[31]. (The actual composition of the structures shown in B50 is likely to be somewhat more enriched in polymer due to crystallisation of a fraction of the PCBM.) B65 exhibits a disordered structure with patchy crystalline domains because the low fraction of P3HT cannot drive self-assembly of an ordered nanostructure.

Self-assembly of the polymer nanostructures is clearly driven by crystallisation of the P3HT block rather than enthalpic repulsions between the blocks. Given the oligomeric nature of the copolymer (N $\equiv$ n + m = 64), a Flory-Huggins interaction parameter, χ = 0.16 would be needed to reach the threshold value of χN = 10.5 for block copolymer microphase separation. That is, the enthalpic repulsion would have to be an order of magnitude greater than for a strongly segregated system (e.g. Poly(styrene-*b*-methylmethacrylate)[32]), which is highly unlikely given the similar chemical structures of the two blocks.

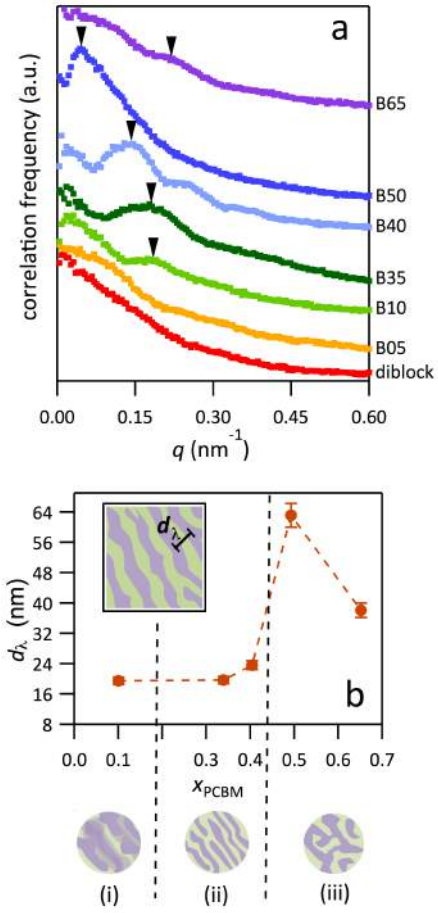

Fig. 6 Block copolymer length scales measured by AFM for P3HT-*b*-P3EHT:PCBM thin films. (a) Radial integrations of the phase image DFT's, arrows denote the peak used to calculate d_λ (b) The repeat domain spacing, d_λ (●). The schematics below the graph correspond to the distinct surface nano-morphologies observed: (i) disordered, (ii) fine, ordered lamellae, and (iii) large, disordered structures.

3.4 Microscopic surface undulations and PCBM crystals

Microscopic surface undulations in the thin film blends result from the addition of PCBM. Fig. 7 shows optical micrographs of the pre- and post-annealed films. Before annealing, the films are smooth ($<$ 0.5 nm root-mean-square roughness), and after annealing the films exhibit height undulations ranging from 10 - 100 nm, on the order of the original thickness of the films. The neat diblock film remains smooth, but the blended samples exhibit surface features ranging from raised beads to film breakup, depending on the PCBM fraction. Crystallisation of the polymer reinforces the undulated surfaces, and upon cooling, they are observed to remain stable for 14 months tested.

The evolution of surface undulations occurs within the first 30 minutes of annealing, simultaneous with PCBM crystallisation, indicating a causal relationship. Specifically, PCBM rods growing out of the plane of the film appear to draw the polymer film up around them by capillary force, as detailed in ESI Fig S11. Blends with a high PCBM content are initially amorphous, as observed in GIWAXS, and more susceptible to liquid-like behaviour due to the low T_g of the polymer (-2°C). Even blends with a PCBM fraction below x_{rod} exhibit small surface undulations due to the reduced number of polymer crystalline domains. Oxidation is known to suppress the growth of PCBM crystals, and consequently no surface undulations were observed for oxidised films (shown in ESI Fig. S15).

ESI Section S1.5 expands upon this mechanism by showing: (i) the time evolution of microstructures in blend B40, (ii) OM and AFM details of the sparse microscopic PCBM crystals in blends above x_{rod}, (iii) AFM details of the modulated polymer surfaces and out-of-plane PCBM crystals, and (iv) the nucleation density of microscopic PCBM crystals in B65.

3.5 General mechanism

We propose a mechanism to explain the evolution of nano- and microstructures in P3HT-*b*-P3EHT:PCBM thin films. The schematics at the bottom of Fig. 7 depict the evolution of structure

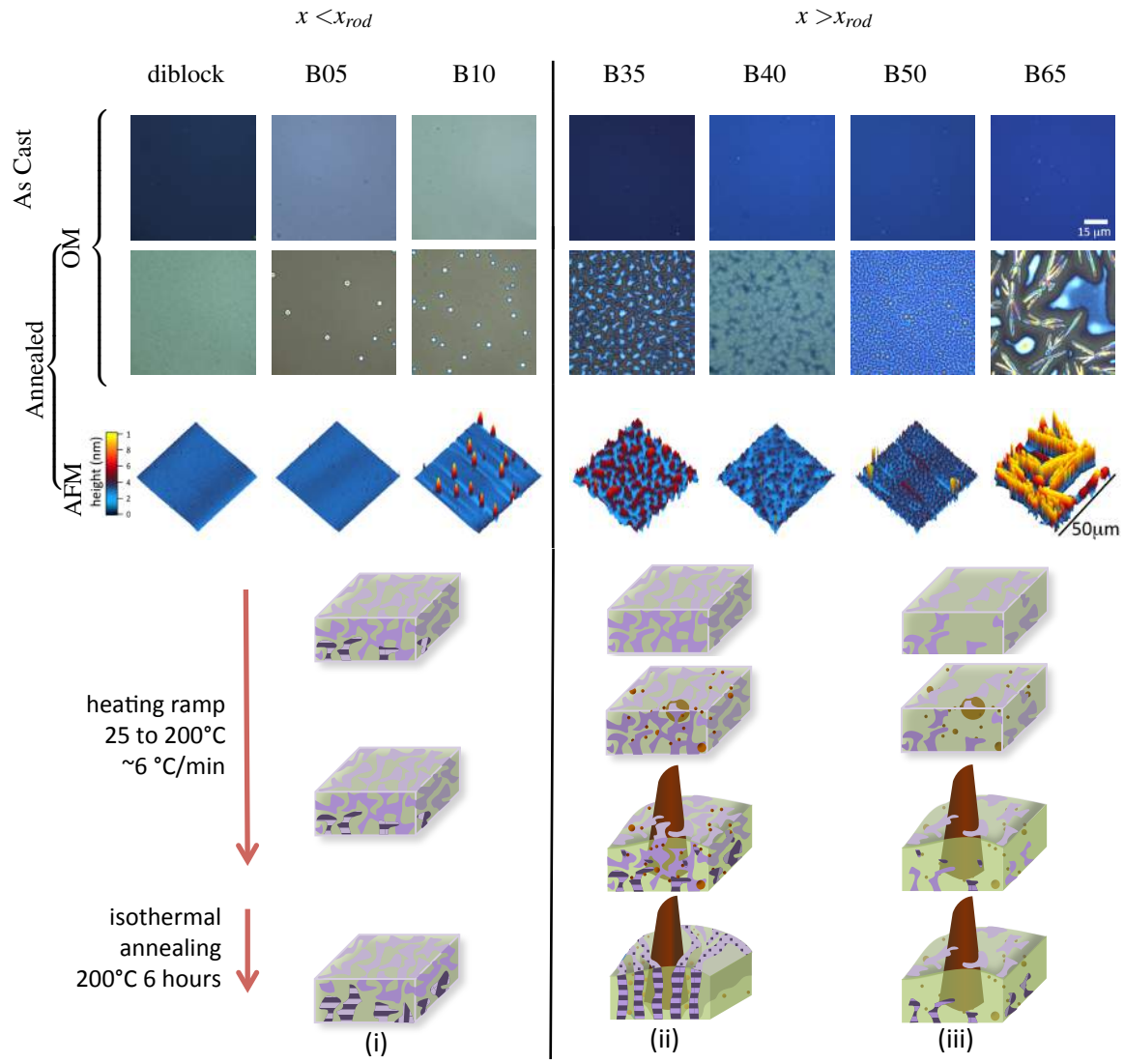

Fig. 7 Microscopic characterisation of P3HT-*b*-P3EHT:PCBM thin films ranging from 0 - 65 wt% PCBM. "As Cast" films were given no thermal treatment and "Annealed" films were heated for 6 hours at 200 °C. The scale bar shown for B65 applies to all images. Topographical AFM images illustrate the height of surface undulations; scans are 50 × 50 μm laterally and the colour map is scaled 0 - 100 nm. Schematics illustrate the structural evolution in thin films for the three ordering regimes observed with AFM. Striped purple regions represent crystalline P3HT, green regions are amorphous P3EHT-rich phases, and brown regions are crystalline PCBM.

for the three cases of film structure defined in Fig. 6.

For case (i) the unannealed film contains a large population of edge-on P3HT crystals that are nucleated when the film is drying (see Fig. 4b). The 6 hour anneal at 200°C is very close to the T_m of P3HT, so the nucleation and growth rates of P3HT crystals are very low. However, the existent crystals are able to partially melt, reorganise, and coarsen. Surface structures observed post-annealing are disordered, with diffuse interfaces between the crystalline and amorphous domains, whilst GI-WAXS indicates that crystal orientation is almost entirely driven by the bottom substrate. Together, these observations suggest poor propagation of the P3HT crystals through the thickness of the film.

For cases (ii) and (iii), the films start with no detectable PCBM crystals. We infer that the degree of P3HT crystallinity is very low from the GIWAXS result that the as-cast diblock copolymer is fully crystallised whilst B65 is fully amorphous (see Fig. 4b). Consequently, these blends start as rubbery films (due to the sub-room temperature T_g's of both polymer blocks), lacking the physical cross links provided by P3HT crystallites. Upon heating, PCBM crystallises rapidly in blends above x_{rod}, competing with the cold crystallisation of P3HT in the copolymer. The fullerene is more mobile than the polymer, forming microscopic crystals within 30 minutes, and causing the surface of the films to undulate. For case (ii), the long anneal allows P3HT crystals to coarsen through the thickness of the film, driving self-assembly of the block copolymer into P3HT- and P3EHT-rich lamellar domains oriented perpendicular to the substrate. Undulations in the film surface do not perturb the self-assembled structure (see ESI Fig. S14). For case (iii) the overall fraction of P3HT is too small to form lamellae propagating through the thickness of the film, and so the structure disorders via an intermediate droplet micro emulsion (B50).

The dramatically improved ordering for blends with $x_{PCBM} > x_{rod}$ implies a cooperativity between PCBM and P3HT crystallisation. PCBM crystals nucleate isotropically throughout the thickness of the film (see ESI Fig. S7a), and most likely act as heterogeneous nucleation sites for P3HT crystals. Upon annealing, these randomly oriented P3HT crystals are able to coarsen through the thickness of the film, directed by the substrate interface. In films with $x_{PCBM} < x_{rod}$, polymer nucleation occurs primarily at the substrate interface, and is less effective at propagating through the film, leading to poorly ordered surface structures.

4 Conclusions

We have produced 20 nm nanostructures in thin films comprising blends of an all-conjugated diblock copolymer, P3HT-*b*-P3EHT, with fullerene PCBM, that are stable to structural ageing for over 14 months. The concentration of PCBM controls the size and shape of polymer nanostructures and the degree of polymer crystallinity. Crystallisation of the P3HT block was observed to drive self-assembly of the otherwise disordered block copolymer. The greatest degree of nano structural order was observed for polymer blends in which PCBM crystallised, suggesting that PCBM crystallites heterogeneously nucleate P3HT crystals. On the basis of our measured observations, we have proposed a general mechanism for the evolution of nano- and macroscopic structures in blended thin films.

5 Acknowledgments

AJN acknowledges support by an Imperial College Junior Research Fellowship and from a Royal Society Research Grant (RG110374). JB and RD are funded under an EPSRC Doctoral Training Centre in Plastic Electronics (grant number EP/G037515/1). JB holds an Industrial Fellowship with the Royal Commission for the Exhibition of 1851. JN thanks the Royal Society for a Wolfson Merit award. JN, AAYG, and MV acknowledge support from the EPSRC via grants EP/G031088/1 and EP/J50002/1 and a Doctoral Training Award. We thank Diamond Light Source for access to

beamline I07 (proposal number SI8339-1) that contributed to the results presented here. We thank Jonathan Rawles for his assistance at I07, Paul Smith for helpful discussions, and Geordie's for inspiration.

References

1 M. Jø rgensen, K. Norrman, S. A. Gevorgyan, T. Tromholt, B. Andreasen and F. C. Krebs, *Advanced Materials*, 2012, **24**, 580–612.

2 R. Tipnis, J. Bernkopf, S. Jia, J. Krieg, S. Li, M. Storch and D. Laird, *Solar Energy Materials and Solar Cells*, 2009, **93**, 442–446.

3 F. S. Bates and G. H. Fredrickson, *Physics Today*, 1999, 32–38.

4 P. D. Topham, A. J. Parnell and R. C. Hiorns, *Journal of Polymer Science Part B: Polymer Physics*, 2011, **49**, 1131–1156.

5 M. He, F. Qiu and Z. Lin, *Journal of Materials Chemistry*, 2011, **21**, 17009–17548.

6 I. W. Hamley, *Advances in Polymer Science*, Springer-Verlag, Berlin, 1999, vol. 148, ch. 10, pp. 113–137.

7 Y.-L. Loo and R. A. Register, *Developments in Block Copolymer Science and Technology*, John Wiley and Sons, Ltd., 2004, ch. 6, pp. 213–243.

8 B. Nandan, J. Hsu and H. Chen, *Journal of Macromolecular Science, Part C: Polymer Reviews*, 2011, **46**, 143–172.

9 P. Rangarajan, R. A. Register, L. J. Fetters, W. Bras, S. Naylor and A. J. Ryan, *Macromolecules*, 1995, **28**, 4932–4938.

10 S. B. Myers and R. A. Register, *Macromolecules*, 2010, **43**, 393–401.

11 D. Gao, J. Hollinger and D. S. Seferos, *ACS Nano*, 2012, **6**, 7114–7121.

12 C. Guo, Y.-H. Lin, M. D. Witman, K. A. Smith, C. Wang, A. Hexemer, J. Strzalka, E. D. Gomez and R. Verduzco, *Nano Letters*, 2013, **13**, 2957–2963.

13 R. H. Lohwasser, G. Gupta, P. Kohn, M. Sommer, A. S. Lang, T. Thurn-Albrecht and M. Thelakkat, *Macromolecules*, 2013, **46**, 4403–4410.

14 Y. Kim, S. Cook, S. M. Tuladhar, S. A. Choulis, J. Nelson, J. R. Durrant, D. D. C. Bradley, M. Giles, I. McCulloch, C.-S. Ha and M. Ree, *Nature Materials*, 2006, **5**, 197–203.

15 W. Yin and M. Dadmun, *ACS Nano*, 2011, **5**, 4756–4768.

16 Y.-L. Loo, R. A. Register and A. J. Ryan, *Macromolecules*, 2002, **35**, 2365–2374.

17 R. S. Loewe, P. C. Ewbank, J. Liu, L. Zhai and R. D. McCullough, *Macromolecules*, 2001, **34**, 4324–4333.

18 V. Ho, B. W. Boudouris and R. A. Segalman, *Macromolecules*, 2010, **43**, 7895–7899.

19 Y. Zhang, K. Tajima and K. Hashimoto, *Macromolecules*, 2009, **42**, 7008–7015.

20 S. Hugger, R. Thomann, T. Heinzel and T. Thurn-Albrecht, *Colloid & Polymer Science*, 2004, **282**, 932–938.

21 C. Müller, C. P. Radano, P. Smith and N. Stingelin-Stutzmann, *Polymer*, 2008, **49**, 3973–3978.

22 J. Balko, R. H. Lohwasser, M. Sommer, M. Thelakkat and T. Thurn-Albrecht, *Macromolecules*, 2013, **46**, 9642–9651.

23 F. P. V. Koch, M. Heeney and P. Smith, *Journal of the American Chemical Society*, 2013, **135**, 13699–709.

24 N. Kayunkid, S. Uttiya and M. Brinkmann, *Macromolecules*, 2010, **43**, 4961–4967.

25 S. Lilliu, T. Agostinelli, E. Pires, M. Hampton, J. Nelson and J. E. Macdonald, *Macromolecules*, 2011, **44**, 2725–2734.

26 T. Agostinelli, S. Lilliu, J. G. Labram, M. Campoy-Quiles, M. Hampton, E. Pires, J. Rawle, O. Bikondoa, D. D. C. Bradley, T. D. Anthopoulos, J. Nelson and J. E. Macdonald, *Advanced Functional Materials*, 2011, **21**, 1701–1708.

27 N. D. Treat, C. G. Shuttle, M. F. Toney, C. J. Hawker and M. L. Chabinyc, *Journal of Materials Chemistry*, 2011, **21**, 15224–15231.

28 P. E. Hopkinson, P. A. Staniec, A. J. Pearson, A. D. F. Dunbar, T. Wang, A. J. Ryan, R. A. L. Jones, D. G. Lidzey and A. M. Donald, *Macromolecules*, 2011, **44**, 2908–2917.

29 M. T. Rispens, A. Meetsma, R. Rittberger, C. J. Brabec, N. S. Sariciftci and J. C. Hummelen, *Chemical Communications*, 2003, 2116–2118.

30 J. Zhao, A. Swinnen, G. Van Assche, J. Manca, D. Vanderzande and B. Van Mele, *The Journal of Physical Chemistry B*, 2009, **113**, 1587–1591.

31 J. Lee, O. H., M. L. Ruegg, N. P. Balsara, Y. Zhu, S. P. Gido, R. Krishnamoorti and M.-H. Kim, *Macromolecules*, 2003, **36**, 6537–6548.

32 N. P. Balsara and H. B. Eitouni, *Physical Properties of Polymer Handbook 2e*, Springer, 2006, ch. 19, pp. 339–356.